AGU PUBLICATIONS

JGR

Journal of Geophysical Research: Space Physics

RESEARCH ARTICLE
10.1002/2015JA022060

Key Points:
- Crustal magnetic fields affect electron densities at higher altitudes, not close to the peak
- Magnetic field inclination appears to have only a marginal affect
- Improved empirical model of the Martian dayside ionosphere developed

Correspondence to:
F. Němec,
frantisek.nemec@gmail.com

Citation:
Němec, F., D. D. Morgan, D. A. Gurnett, and D. J. Andrews (2016), Empirical model of the Martian dayside ionosphere: Effects of crustal magnetic fields and solar ionizing flux at higher altitudes, *J. Geophys. Res. Space Physics*, *121*, 1760–1771, doi:10.1002/2015JA022060.

Received 20 OCT 2015
Accepted 29 JAN 2016
Accepted article online 2 FEB 2016
Published online 23 FEB 2016

Empirical model of the Martian dayside ionosphere: Effects of crustal magnetic fields and solar ionizing flux at higher altitudes

F. Němec[1], D. D. Morgan[2], D. A. Gurnett[2], and D. J. Andrews[3]

[1]Faculty of Mathematics and Physics, Charles University in Prague, Prague, Czech Republic, [2]Department of Physics and Astronomy, University of Iowa, Iowa City, Iowa, USA, [3]Swedish Institute of Space Physics, Uppsala, Sweden

Abstract We use electron density profiles measured by the Mars Advanced Radar for Subsurface and Ionosphere Sounding instrument on board the Mars Express spacecraft to investigate the effects of possible controlling parameters unconsidered in the empirical model of Němec et al. (2011, hereafter N11). Specifically, we focus on the effects of crustal magnetic fields and $F_{10.7}$ proxy of the solar ionizing flux at higher altitudes. It is shown that while peak electron densities are nearly unaffected by crustal magnetic fields, electron densities at higher altitudes are significantly increased in areas of stronger magnetic fields. The magnetic field inclination appears to have only a marginal effect. Moreover, while the N11 empirical model accounted for the variable solar ionizing flux at low altitudes, the high-altitude diffusive region was parameterized only by the solar zenith angle and the altitude. It is shown that this can lead to considerable inaccuracies. A simple correction of the N11 model, which takes into account both the crustal magnetic field magnitude and the effect of $F_{10.7}$ at higher altitudes, is suggested.

1. Introduction

The amount of the electron density data from the dayside Martian ionosphere is nowadays considerably large. Entire electron density profiles (i.e., electron densities as a continuous function of the altitude) were obtained using radio occultation experiments from the Mars Global Surveyor (MGS) [*Hinson et al.*, 1999] and Mars Express satellites [*Pätzold et al.*, 2005; *Grandin et al.*, 2014]. Moreover, the Mars Advanced Radar for Subsurface and Ionosphere Sounding (MARSIS) in the active ionosphere sounder (AIS) mode provides electron density profiles from the spacecraft altitude down to the altitude of the peak electron density in the ionosphere [*Gurnett et al.*, 2005; *Morgan et al.*, 2008; *Sánchez-Cano et al.*, 2012; *Morgan et al.*, 2013]. Since August 2005, the MARSIS instrument provided more than 100,000 electron density profiles. The main advantage of these profiles as compared to the radio occultation data is that their spatial coverage is not restricted by geometric constraints imposed by the orbits of Earth and Mars [*Tyler et al.*, 2001; *Withers and Mendillo*, 2005]. This makes them favorable for the specification of global morphologies [*Mendillo et al.*, 2013].

The large set of experimental electron density data, along with a basic understanding of physical processes taking place, can be used to construct efficient simple empirical models of the Martian ionosphere. These models typically make use of a classical Chapman theory [*Chapman*, 1931a, 1931b]. Although this theory takes into account only photoionization and recombination, neglecting, among other things, and any plasma transport, it performs surprisingly well at altitudes close to the altitude of the ionospheric peak [*Gurnett et al.*, 2005, 2008; *Morgan et al.*, 2008; *Withers*, 2009]. *Mendillo et al.* [2013] used nearly 113,000 peak electron density values obtained from 2005 to 2012 by the MARSIS instrument to develop a model of peak electron densities in the dayside Martian ionosphere parameterized by the solar zenith angle (SZA), orbital distance, and $F_{10.7}$ proxy of the solar ionizing flux. The same parameterization and a combined data set of 1200 MARSIS AIS profiles and 500 MGS radio occultation profiles were used by *Sánchez-Cano et al.* [2013] to develop an empirical model of electron density profiles. The model included not only the main M2 ionospheric layer but also the lower M1 layer [*Schunk and Nagy*, 2009; *Fox and Yeager*, 2009; *Fox and Weber*, 2012; *Fallows et al.*, 2015a, 2015b].

Němec et al. [2011] used 30,283 MARSIS AIS profiles and nearly 200,000 local measurements of electron density acquired at SZAs less than 100° to construct a model of dayside electron densities at altitudes above the altitude of the peak electron density (N11 model). Two different altitudinal regions were distinguished.

Electron densities at altitudes up to about 5 neutral scale heights above the peak altitude were described according to the Chapman theory. Electron densities at altitudes higher than about 10 neutral scale heights above the peak altitude were found to decrease exponentially with the altitude, consistent with the upward plasma diffusion and with the results obtained by *Duru et al.* [2008, 2011]. A smooth transition between the two dependencies was used to interpolate the electron densities at intermediate altitudes.

Although the N11 model performs overall reasonably well, it did not take into account two possibly important controlling parameters: (i) crustal magnetic fields and (ii) variable solar ionizing flux in the high-altitude (diffusion controlled) region. We use a large number of electron density profiles acquired by the MARSIS instrument since August 2005 until the end of 2013 to identify the influence of parameters unconsidered in the N11 model. Specifically, we focus on the effects of crustal magnetic fields and $F_{10.7}$ proxy for the solar ionizing flux at higher altitudes. The obtained relationships are used to suggest an improvement of the N11 model.

The used data set is described in section 2. A comparison of the measured data with the N11 model and a possible model improvement are presented in section 3. The obtained results are discussed in section 4. Section 5 contains a brief summary.

2. Data Set

Electron density profiles obtained by the MARSIS instrument on board the Mars Express spacecraft have been used. In the beginning of the mission, the spacecraft was orbiting Mars at an eccentric orbit with a periapsis altitude of about 275 km, an apoapsis altitude of about 10,100 km, an inclination of 86°, and an orbital period of 6.75 h [*Chicarro et al.*, 2004]. The spacecraft orbit slightly evolves during the duration of the mission, more current orbital values are the periapsis altitude of about 380 km, the apoapsis altitude of about 10,500 km, and the orbital period of 7 h. A 40 m long electric dipole antenna is used for transmitting a sounding wave and a subsequent reception of its reflection from the ionosphere. During the ionospheric sounding the transmitter steps through 160 quasi-logarithmically spaced frequencies from 0.1 to 5.5 MHz ($\Delta f/f \approx 0.02$). The echoes are recorded in 80 equally spaced time delay bins over an interval of 7.31 ms. More details about the MARSIS instrument can be found in *Picardi et al.* [2004] and *Jordan et al.* [2009]. The inversion techniques applied to the measured ionospheric traces, i.e., the way of their conversion to electron density profiles, were described in detail by *Morgan et al.* [2008, 2013]. The main idea will here be briefly described; the references given above provide more detail.

The principal output of the MARSIS instrument is called an ionogram. It is the intensity of detected echoes as a function of the frequency f and the time delay Δt. The basic idea of the ionospheric sounding is that the detected intensity is enhanced at frequencies and time delays which correspond to the signal reflection from the ionosphere [*Gurnett et al.*, 2005]. This feature is called "ionospheric trace." It spans up to the frequency equal to the peak electron plasma frequency in the ionosphere (higher frequencies are not reflected by the ionosphere), and it allows us to determine electron density profiles spanning from the spacecraft altitude down to the altitude of the peak electron density in the ionosphere.

During the calculation it is assumed that the electron density decreases monotonically with the altitude. This is typically the case, except for occasionally occurring transient layers [*Kopf et al.*, 2008] and other atypical features [*Withers et al.*, 2005, 2012]. In order to avoid these, we use only the ionospheric traces with the jump in the delay time between adjacent data points lower than 0.2 ms, i.e., we avoid the traces which contain noticeable cusps. Another assumption made during the inversion procedure is that the altitudinal dependence of the electron density is exponential between the altitudes where two adjacent sounding frequencies are reflected. If the two adjacent sounding frequencies were not close to each other, this might result in significant inaccuracies. We have thus selected only the ionospheric traces with the frequency gaps between adjacent sounding frequencies lower than 0.4 MHz.

Finally, one has to deal with problems related to the low-frequency part of the ionospheric trace. Specifically, the sounding signal at low frequencies is too weak to be detected, i.e., the electron densities lower than about 10^4 cm^{-3} cannot be typically detected by the ionospheric sounding [*Němec et al.*, 2010]. It is, however, possible to determine the local electron density at the spacecraft location from the analysis of enhanced intensities at frequencies corresponding to the harmonics of the local electron plasma frequency [*Duru et al.*, 2008, 2011; *Andrews et al.*, 2013]. When doing the ionospheric inversion, it is then necessary to interpolate the electron density profile between the spacecraft location and the altitude corresponding to the lowest-frequency data

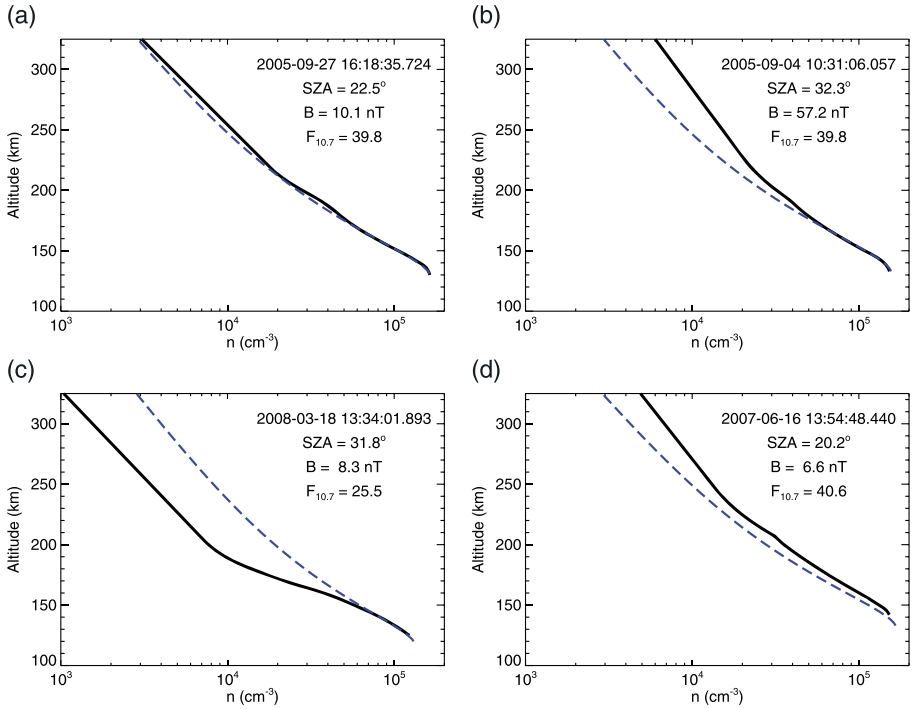

Figure 1. (a–d) Examples of electron density profiles measured by the MARSIS instrument are shown by the black curves. The times of the measurements, solar zenith angles, and magnitudes of the crustal magnetic field calculated using the *Cain et al.* [2003] magnetic field model at an altitude of 400 km and $F_{10.7}$ proxies of the solar ionizing flux are given at the upper rights. Model electron density profiles calculated using the N11 model for the appropriate conditions are shown by the dashed blue curves.

point from the ionospheric sounding. We select only the ionospheric traces for which the altitudinal range of this interpolation is reasonably small. Specifically, we require that the logarithmic range of the frequency gap between the plasma frequency at the spacecraft location and the lowest-frequency data point from the ionospheric sounding is lower than the logarithmic frequency range of the ionospheric trace itself. In other words, on the logarithmic scale, the low-frequency data gap is required to be lower than the data range of the ionospheric trace. Although this ensures that the selected traces are those for which the ionospheric inversion can be considered as highly accurate, it also introduces a selection bias in our data set, as we preferentially select the ionospheric traces with high electron densities at the spacecraft location.

In order to reduce this selection effect and in order to prevent the interpolation at the lowest frequencies to span over a large altitudinal range, we select only electron density profiles obtained at spacecraft altitudes lower than 450 km. Moreover, as no information about electron densities is available at altitudes higher than the spacecraft altitude, and we want to analyze electron density profiles up to the altitude of 325 km (the z_0^{dif} altitude of the N11 model), we select only electron density profiles obtained at spacecraft altitudes higher than 325 km. Finally, as the aim is to analyze only the dayside ionosphere controlled primarily by the solar ionizing flux, only electron density profiles obtained at SZAs lower than 80° are used. This ensures that our data set is not influenced by day-night transition effects [*Girazian and Withers*, 2013]. We note that within this range of SZAs the N11 model assumes principally a constant electron density of $n_0^{\mathrm{dif}} = 2800\ \mathrm{cm}^{-3}$ at an altitude of 325 km. All the aforementioned selection criteria leave us with 12,665 electron density profiles measured since August 2005 until the end of 2013.

Examples of electron density profiles obtained by the MARSIS instrument are shown in Figure 1 by the black curves. The times of the measurements, SZAs, and crustal magnetic field magnitudes calculated using the *Cain et al.* [2003] magnetic field model at an altitude of 400 km and $F_{10.7}$ proxies of the solar ionizing flux are given at the upper rights of individual panels. Further, the blue dashed lines in Figure 1 show model electron density profiles calculated using the N11 model for the appropriate conditions. The four examples shown in Figures 1a–1d represent four typical situations which may occur. Figure 1a shows an example where the model and measured profiles agree well, both close to the ionospheric peak and at higher altitudes.

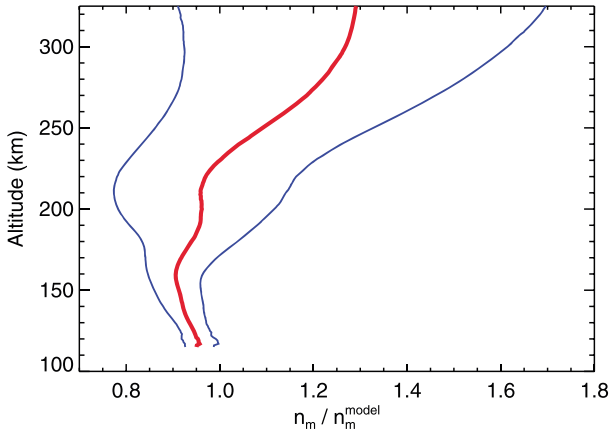

Figure 2. Ratio of measured to model electron density profiles. The median ratio is shown by the red curve, and the blue curves correspond to 0.25 and 0.75 quartiles.

Figure 1b shows an example of a situation where the model profile corresponds to the measured profile close to the ionospheric peak, but it underestimates the electron densities at higher altitudes. It is noteworthy that this electron density profile was measured in the region with exceptionally strong crustal magnetic fields. On the other hand, Figure 1c shows an example of a situation where the model profile corresponds to the measured profile close to the ionospheric peak, but it overestimates the electron densities at higher altitude. It is noteworthy that this electron density profile was measured at the time of extremely low values of $F_{10.7}$ proxy of the solar ionizing flux. Finally, Figure 1d shows an example of a situation where the model profile differs from the measured profile both close to the ionospheric peak and at higher altitudes. We note that all four profiles shown in Figure 1 were measured at SZAs between 20 and 32.5°.

3. Results

In order to analyze a possible influence of the parameters not considered in the N11 model, we use a similar approach as previously employed by *Andrews et al.* [2015]. The idea is that instead of analyzing the measured electron densities themselves, we analyze the ratio between measured electron densities and the electron densities predicted by the N11 model. Such a comparison is, however, problematic at times when the observed peak altitude is (even slightly) different than the model peak altitude. We therefore explicitly shift the peak altitude of the N11 model to be equal to the measured peak altitude, and we force the model to calculate the electron density profiles corresponding to such a situation. Considering that the peak altitude in the N11 model is normally determined from empirical fits, the used approach is reasonable, as it simply replaces the average-fitted value by the value actually measured.

The resulting ratio of measured to model electron density profiles is shown in Figure 2. The red curve shows the median profile ratio, and the blue curves correspond to 0.25 and 0.75 quartiles. It should be noted that as the radar sounding is limited only to altitudes above the peak altitude, only few electron density profiles (those with the lowest peak altitudes) contribute to the lowest altitude portion of the profile ratios. In order to prevent the calculation of median/quartile values from an unreasonably low number of profiles, they are evaluated only at altitudes with at least 100 profiles. This limit on the minimum number of profiles to be used for calculating the median and quartile values is used throughout the paper.

It can be seen that at the altitudes close to the peak the obtained ratios are close to 1. However, the measured electron densities tend to be somewhat lower than the model electron densities. This has two principal reasons. First, the data coverage is rather different than the one used when constructing the N11 model. The newly added data were obtained during an ascending phase of the solar cycle. Also, the data coverage with respect to crustal magnetic fields was quite different. Second, while the N11 model parameters at altitudes close to the peak were based on Chapman fits of measured electron density profiles, the measured electron density profiles used in this paper were directly evaluated from the ionospheric traces. Taking into account that the two consecutive sounding frequencies differ by about 2%, the directly evaluated peak electron

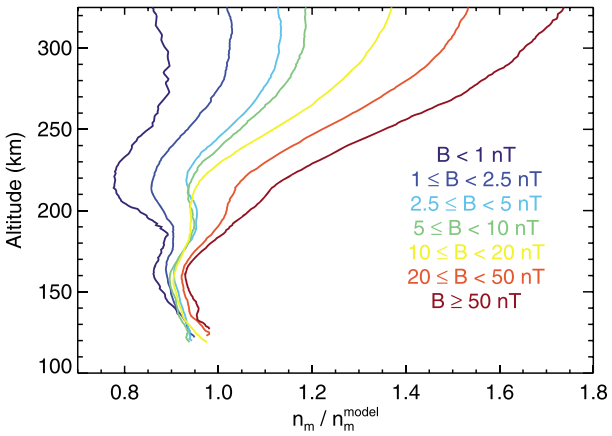

Figure 3. Median ratios of measured to model electron density profiles calculated for various crustal magnetic field magnitudes *B*. The magnetic field magnitudes were calculated using *Cain et al.* [2003] magnetic field model at an altitude of 400 km. The individual curves were obtained for $B < 1$ nT, 1 nT $\le B < 2.5$ nT, 2.5 nT $\le B < 5$ nT, 5 nT $\le B < 10$ nT, 10 nT $\le B < 20$ nT, 20 nT $\le B < 50$ nT, and $B \ge 50$ nT, dark blue to dark red, respectively, following the legend at the bottom right.

density is in general underestimated by as much as 4%. However, overall, the measured electron densities at altitudes close to the peak are in a reasonable agreement with the N11 model results, and even the scatter of the distribution expressed by the 0.25 and 0.75 quartiles is rather low.

The scatter of measured to model electron density ratios increases at higher altitudes. The median values, however, remain close to 1 up to an altitude of about 225 km. At altitudes above about 225 km the measured electron densities are systematically larger than the model electron densities (by about 29% at an altitude of 325 km). This increase is partly related to a different data coverage with respect to the parameters unconsidered in the N11 model. Partly, the exponential interpolation of the electron density profile between the spacecraft location and the altitude corresponding to the lowest-frequency data point from the ionospheric sounding may overestimate densities at these altitudes. However, this effect is minimized by the applied criteria on the logarithmic frequency range of the data gap and the spacecraft altitude (section 2). Finally, there is the aforementioned selection bias due to the criteria imposed on the measured ionospheric traces. Specifically, the preferential selection of ionospheric traces with high plasma frequencies at the spacecraft location leads to above-average electron densities at higher altitudes. This would be a problem if these traces were used to determine typical densities. Nevertheless, our aim is to determine the influence of possible additional control parameters not considered in the N11 model, and for this purpose the measured electron density profiles are perfectly suitable.

The first parameter not considered in the N11 model, but influencing electron densities, is the magnitude of the crustal magnetic fields. The results obtained by *Andrews et al.* [2013, 2015] using local electron density measurements at the spacecraft locations showed that on the dayside the plasma density is substantially higher in regions of stronger crustal magnetic fields. These results were, however, limited only to the higher altitudes sampled regularly by the Mars Express spacecraft (above about 300 km). Electron density profiles obtained by the radar sounding allow us to investigate the magnetic field influence down to the peak altitudes.

Figure 3 shows the median ratios of measured to model electron density profiles calculated for various crustal magnetic field magnitudes *B*. The magnetic field magnitudes were calculated using the *Cain et al.* [2003] magnetic field model at an altitude of 400 km, as is the case throughout the present paper. The altitude of 400 km was chosen, because it is the altitude of the magnetic field measurements which were used when constructing the *Cain et al.* [2003] magnetic field model. Other choices of the altitude where the magnetic field model is evaluated lead, however, to very similar results (not shown). The individual curves were obtained for $B < 1$ nT, 1 nT $\le B < 2.5$ nT, 2.5 nT $\le B < 5$ nT, 5 nT $\le B < 10$ nT, 10 nT $\le B < 20$ nT, 20 nT $\le B < 50$ nT, and $B \ge 50$ nT, dark blue to dark red, respectively, following the legend at the bottom right. It can be seen that the electron densities measured in areas with stronger crustal magnetic fields are systematically larger than the electron densities measured in areas with weaker crustal magnetic fields. Although this trend is rather weak and disputable at the altitudes close to the peak, it becomes well pronounced at altitudes higher than about 200 km. The difference is as high as a factor of 2 at an altitude of 325 km.

The influence of the crustal magnetic field magnitude at two chosen altitudes, the peak altitude and the altitude of 325 km, is investigated more in detail in Figure 4. Measured to model peak electron densities as a function of the crustal magnetic fields are shown by black points in Figure 4a. The horizontal red lines show the median values calculated over given intervals, and the horizontal blue lines show 0.25 and 0.75 quartiles.

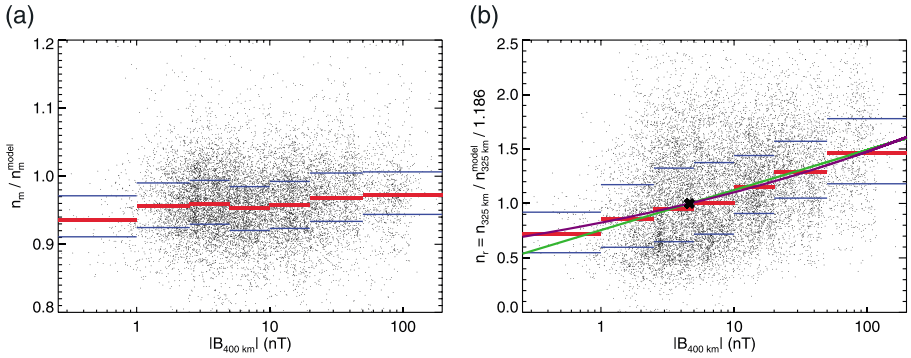

Figure 4. (a) Measured to model peak electron densities as a function of the crustal magnetic field magnitude at an altitude of 400 km [*Cain et al.*, 2003]. The horizontal red lines show the median values calculated over given intervals, and the horizontal blue lines show 0.25 and 0.75 quartiles. (b) Measured to model electron densities (with the normalization applied) at an altitude of 325 km as a function of the crustal magnetic field magnitude at an altitude of 400 km [*Cain et al.*, 2003]. The red and blue horizontal lines correspond to median and 0.25 and 0.75 quartiles, respectively. The black cross corresponds to the point $[B_0, 1]$ (see text). The purple curve shows the best fit according to $n_r = (B/B_0)^k$. The green line shows the best fit according to $n_r = 1 + a \log_{10}(B/B_0)$.

It can be seen that the crustal magnetic field magnitude influence on the peak electron densities is rather weak. The value of the Spearman's rank correlation coefficient is only about 0.07, but the statistical significance is principally 100% (significance level less than 10^{-6}). The magnetic field influence, however, starts to be an important parameter at higher altitudes, as it is demonstrated in Figure 4b, which was obtained for an altitude of 325 km.

In order to account for the aforementioned selection bias in the used data set, the measured to model electron densities were normalized by their median. However, the used data set covers a different range of parameters than the data set used for the construction of the N11 model: the median values of B and $F_{10.7}$ parameters in the present data set are about 7.132 nT and 36.97×10^{-22} W m^{-2} Hz^{-1}, while the median values of these parameters in the data set used for the construction of the N11 model were about $B_0 = 4.634$ nT and $F_{10.7(0)} = 35.3133 \times 10^{-22}$ W m^{-2} Hz^{-1}, respectively. It is thus reasonable to normalize by the median electron density calculated only from the profiles with parameters close to the median values of the N11 data set. Assuming that the main parameters are B and $F_{10.7}$, only the profiles with B within 1 nT from B_0 and $F_{10.7}$ within 3×10^{-22} W m^{-2} Hz^{-1} from $F_{10.7(0)}$ were used for the calculation. The resulting median value used for normalization is about 1.186. This corresponds to the factor by which our data set typically overestimates the electron densities at an altitude of 325 km due to the selection bias. We note that this normalization ensures that the corrected (i.e., after the normalization) measured to model electron densities n_r at an altitude of 325 km are close to 1 for electron density profile areas with $B \approx B_0$ and $F_{10.7} \approx F_{10.7(0)}$.

Ratios of measured to model electron densities with the normalization applied obtained for an altitude of 325 km, $n_r = n_{325\mathrm{km}}/n_{325\mathrm{km}}^{\mathrm{model}}/1.186$, are shown as a function of B by black points in Figure 4b. The red and blue horizontal lines correspond to median and 0.25 and 0.75 quartiles, respectively. It can be seen that the black cross corresponding to the point $[B_0, 1]$ lies close to the center of the measured distribution, as expected. The electron density ratios clearly increase with B. The value of the Spearman's rank correlation in this case is about 0.35.

The effect of crustal magnetic field magnitude at low altitudes is low as compared to the scatter of the data points, i.e., it does not make sense to account for it in the N11 model, as it would not much improve the overall model performance. However, when modeling the electron densities at higher altitudes, the effect of the crustal magnetic field magnitude should be accounted for. Considering the shape of the dependence in Figure 4b and the fact that the dependence $n_r(B)$ should, by definition, go through the point $[B_0, 1]$, we consider two simple dependencies to fit the observations

$$n_r = \left(\frac{B}{B_0}\right)^k \tag{1}$$

$$n_r = 1 + a \log_{10}(B/B_0) \tag{2}$$

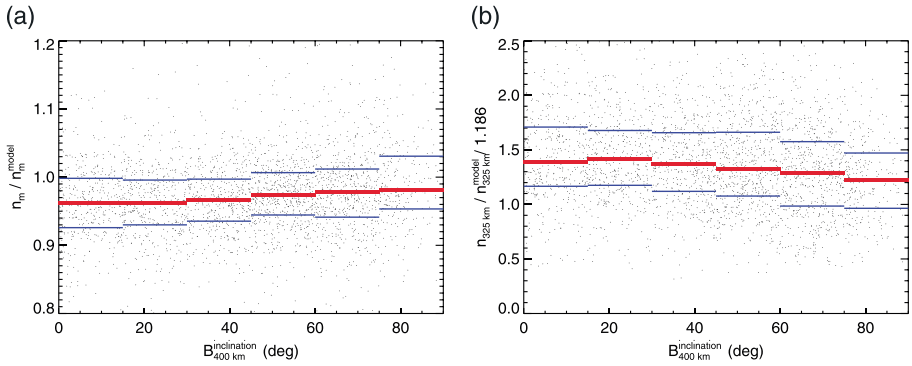

Figure 5. Measured to model electron densities as a function of the crustal magnetic field inclination at an altitude of 400 km [*Cain et al.*, 2003]. (a) Results obtained for peak electron densities. (b) Results obtained for corrected electron densities at an altitude of 325 km. The red and blue horizontal lines correspond to median and 0.25 and 0.75 quartiles, respectively.

The purple curve shows the best fit according to equation (1), which results in $k = 0.127$. The green curve shows the best fit according to equation (2), which results in $a = 0.368$. It can be seen although there is not a large difference between the two curves; the purple curve performs slightly better, particularly at low values of B.

Having shown that the magnitude of crustal magnetic fields can significantly affect ionospheric electron densities, it is of interest to determine the influence of the magnetic field inclination. In other words, whether the electron densities are different in the areas with horizontal crustal magnetic fields (magnetic field inclination equal to 0°) than in the areas with vertical crustal magnetic fields (magnetic field inclination equal to 90°). This is investigated in Figure 5, using the same format as in Figure 4. Only the areas with $B \geq 20$ nT were selected for the analysis, as it does not make sense to evaluate the magnetic field inclination in the areas where the crustal magnetic fields are not sufficiently strong. Figure 5a shows the measured to model peak electron densities as a function of the magnetic field inclination. It can be seen that peak electron densities are somewhat larger in the areas of more inclined crustal magnetic fields, but the effect is rather weak. The value of the Spearman's rank correlation coefficient is about 0.14. Figure 5b shows that the trend at an altitude of 325 km is rather different. Electron densities at these altitudes are slightly lower in areas with high crustal magnetic field inclination. The value of the Spearman's rank correlation is about −0.14. Both these trends are statistically significant (principally 100%, significance level less than 10^{-6}). However, the statistical significance stems from the large number of included data points. The trends themselves are weak as compared to the scatter of individual data points, i.e., their inclusion in the N11 model would not significantly alter the model performance.

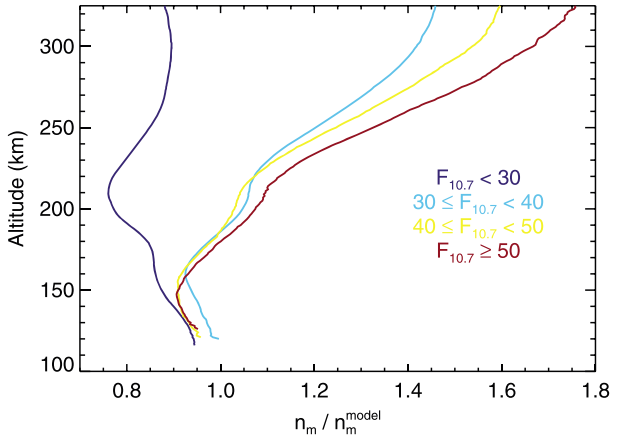

Figure 6. Median ratios of measured to model electron density profiles calculated for various values of $F_{10.7}$. The individual curves were obtained for $F_{10.7} < 30 \times 10^{-22}$ W m^{-2} Hz^{-1}, 30×10^{-22} W m^{-2} Hz^{-1} $\leq F_{10.7} < 40 \times 10^{-22}$ W m^{-2} Hz^{-1}, 40×10^{-22} W m^{-2} Hz^{-1} $\leq F_{10.7} < 50 \times 10^{-22}$ W m^{-2} Hz^{-1}, and $F_{10.7} \geq 50 \times 10^{-22}$ W m^{-2} Hz^{-1}, dark blue to dark red, respectively, following the legend at the bottom right.

Figure 6 uses the same format as Figure 3 to analyze the N11 model performance as a function of $F_{10.7}$. The values of $F_{10.7}$ were determined from the values of $F_{10.7}$ measured at Earth, assuming the $1/r^2$ dependence and taking into account the variable Sun-Mars distance. The orbital longitude separation along with the solar rotation period was used to determine the terrestrial dates most appropriate for the effective $F_{10.7}$ to use at the time of an observation at Mars. A weighted average of two relevant $F_{10.7}$ values (just before and just after) was used [*Morgan et al.*, 2008]. The individual curves in Figure 6

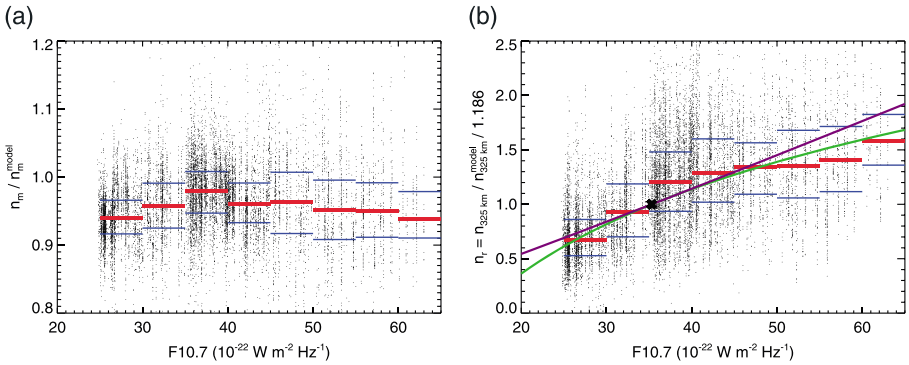

Figure 7. Measured to model electron densities as a function of $F_{10.7}$. (a) Results obtained for peak electron densities. (b) Results obtained for corrected electron densities at an altitude of 325 km. The red and blue horizontal lines correspond to median and 0.25 and 0.75 quartiles, respectively. The black cross corresponds to the point $[F_{10.7(0)}, 1]$ (see text). The purple curve shows the best fit according to $n_r = (F_{10.7}/F_{10.7(0)})^k$. The green line shows the best fit according to $n_r = 1 + a \log_{10}(F_{10.7}/F_{10.7(0)})$.

were obtained for $F_{10.7} < 30 \times 10^{-22}$ W m^{-2} Hz^{-1}, 30×10^{-22} W m^{-2} Hz^{-1} $\leq F_{10.7} < 40 \times 10^{-22}$ W m^{-2} Hz^{-1}, 40×10^{-22} W m^{-2} Hz^{-1} $\leq F_{10.7} < 50 \times 10^{-22}$ W m^{-2} Hz^{-1}, and $F_{10.7} \geq 50 \times 10^{-22}$ W m^{-2} Hz^{-1}, dark blue to dark red, respectively, following the legend at the bottom right. It can be seen that while all the curves are close to each other at altitudes close to the peak altitude, there is a systematic trend of higher measured electron densities at times of higher $F_{10.7}$ at higher altitudes. This might be expected, as the higher solar ionizing flux should clearly result in higher electron densities not only close to the peak altitude (as considered in the N11 model) but also at higher altitudes.

Figure 7 uses the same format as Figure 4 to analyze the effect of $F_{10.7}$ in more detail. Figure 7a shows the measured to model peak electron densities as a function of $F_{10.7}$. There is no strong trend identifiable in the figure, demonstrating that the N11 model accounts well for variable values of $F_{10.7}$ at peak altitudes. Figure 7b shows measured to model electron densities n_r at an altitude of 325 km as a function of $F_{10.7}$. The same normalization as in Figure 4b was used. There is a clear trend of higher electron density ratios at times of higher $F_{10.7}$, consistent with the results depicted in Figure 6. The value of the Spearman's rank correlation coefficient is about 0.55. The trend becomes less pronounced at higher values of $F_{10.7}$, which is possibly related to $F_{10.7}$ not being an ideal proxy of the solar ionizing flux, especially at times of high $F_{10.7}$ [*Mendillo et al.*, 2013; *Girazian and Withers*, 2013].

Considering the shape of the dependence in Figure 7b and taking into account that the dependence $n_r(F_{10.7})$ should, by definition, go through the point $[F_{10.7(0)}, 1]$, we use the same fitting curves as for the magnetic field, i.e., equations (1) and (2) with the substitution $B_0 \rightarrow F_{10.7(0)}$ and $B \rightarrow F_{10.7}$. The purple curve shows the best fit according to equation (1), which results in $k = 1.071$. The green curve shows the best fit according to equation (2), which results in $a = 2.582$. The two curves are roughly comparable, but the green curve performs slightly better, particularly at low/large values of $F_{10.7}$. We note, however, that this fit is clearly unphysical in the sense that the values obtained for low $F_{10.7}$ get negative. However, given the range of $F_{10.7}$ encountered at Mars, it is a simple good fit of the available experimental data.

The fitted dependencies from Figures 4b and 7b can be used to adjust the N11 model in order to account for the previously unconsidered variations with B and $F_{10.7}$. Since the need for improving the model is primarily at higher altitudes, a natural choice is to modify the n_0^{dif} parameter used in the N11 model [*Němec et al.*, 2011, equation (8)]. This parameter has the meaning of the electron density in the "diffusion region" at an altitude of 325 km, and it can be directly adjusted using the obtained fit results. Specifically, we suggest to multiply n_0^{dif} by the following two factors:

$$\alpha_B = \left(\frac{B}{B_0}\right)^k = \left(\frac{B}{4.634\,\mathrm{nT}}\right)^{0.127} \tag{3}$$

$$\alpha_{F_{10.7}} = 1 + a \log_{10} \frac{F_{10.7}}{F_{10.7(0)}} = 1 + 2.582 \log_{10} \frac{F_{10.7}}{35.3133 \times 10^{-22}\,\mathrm{W\,m^{-2}\,Hz^{-1}}} \tag{4}$$

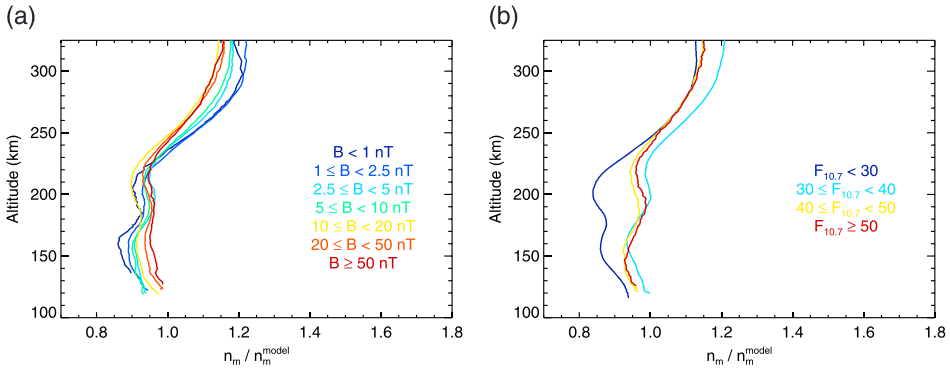

Figure 8. (a) Median ratios of measured to model electron density profiles calculated for various crustal magnetic field magnitudes *B*. The format is the same as in Figure 3. This time, however, the N11 model with the recently suggested improvements was used. (b) Median ratios of measured to model density profiles calculated for various values of $F_{10.7}$. The format is the same as in Figure 6. This time, however, the N11 model with the recently suggested improvements was used.

Figure 8 uses the same format as Figures 3 and 6. However, this time, the measured electron density profiles were normalized by the electron densities calculated using the N11 model improved according to equations (3) and (4). It can be seen in Figure 8a that the normalized electron density profiles obtained in areas with various *B* are nearly on top of each other (within 10% at all analyzed altitudes). The correction for the influence of the crustal magnetic field magnitude thus works extremely well. Figure 8b shows that the scatter of the normalized profiles for various levels of $F_{10.7}$ is slightly larger than the scatter obtained for various levels of *B*. However, the suggested correction still performs very well. The suggested improvement of the N11 model thus seems to account well for the controlling effects of both the crustal magnetic field magnitude and $F_{10.7}$.

4. Discussion

Although the amount of the MARSIS dayside electron density data is quite enormous, they are mostly limited to altitudes close to (and strictly above) the peak altitude. This is due to smaller electron densities being generally difficult to measure, except for the local electron density measurements. These, on the other hand, have rather sparse spatial coverage, as they are only single-point measurements. We used a careful selection of the MARSIS AIS ionospheric traces to obtain a set of the electron density profiles, which cover reliably the altitudinal range up to 325 km. The used profile selection, however, leads to a sampling bias of higher electron densities at higher altitudes. We accounted for this bias by comparing the measured electron densities at an altitude of 325 km with the long-term average electron densities of the N11 model (without the sampling bias). In this way we obtained a unique data set of 12,665 electron densities at an altitude of 325 km, along with the corresponding electron density profiles spanning down the peak altitude. Although no such normalization was done at other altitudes, the analysis of the electron density profiles allowed us to investigate the influence of both the crustal magnetic fields and $F_{10.7}$ at all altitudes between the peak altitude and the altitude of 325 km.

Crustal magnetic fields were found to have only marginal effects on electron densities close to the peak altitude. This is consistent with the results obtained by *Mendillo et al.* [2011], and it is likely explainable by the local production of the plasma by photoionization with the plasma transport being negligible at these altitudes. The slightly larger peak electron densities in areas with larger crustal magnetic field magnitudes can be possibly explained by larger electron temperatures in these regions [*Breus et al.*, 2004; *Nielsen et al.*, 2007a; *Cui et al.*, 2015] due to the local plasma processes [*Gurnett et al.*, 2005; *Duru et al.*, 2006; *Nielsen et al.*, 2007b]. The higher plasma temperatures then, in turn, lead to slower plasma recombination [e.g., *Withers*, 2009, and the references therein] and thus larger plasma densities. The fact that the peak electron densities are somewhat larger in areas with vertical crustal magnetic fields seems to be consistent with this picture [*Gurnett et al.*, 2005; *Duru et al.*, 2006; *Nielsen et al.*, 2007b]. Moreover, localized electrodynamic effects due to ionospheric dynamo processes take place in areas of strong crustal magnetic fields and alter the ionospheric behavior [*Withers et al.*, 2005; *Riousset et al.*, 2014]. However, the effect of the crustal magnetic fields on the electron

densities at altitudes close to the peak altitude is overall small compared to typical N11 model inaccuracies, i.e., including the crustal magnetic field effects would not significantly alter the model performance close to the peak altitude.

The situation is rather different at higher altitudes, where electron densities are systematically affected by the crustal magnetic fields. The electron densities at an altitude of 325 km are by a factor of about 2 larger in areas of strong crustal magnetic fields than in areas of weak crustal magnetic fields. This is consistent with the results obtained by *Andrews et al.* [2013, 2015] who used local electron density measurements at altitudes higher than about 300 km. As for the effect of the magnetic field inclination, there is likely an interplay between the vertical and horizontal transport [*Andrews et al.*, 2013; *Matta et al.*, 2015]. Noting that the draped interplanetary magnetic field is predominantly horizontal relative to the spherical surface on the dayside [*Brain et al.*, 2003; *Nagy et al.*, 2004], the vertical transport is significantly reduced in the areas with weak or nearly horizontal crustal magnetic fields. On the other hand, highly inclined strong crustal magnetic fields allow for a relatively more efficient vertical transport, but they, at the same time, inhibit the horizontal transport. The proper evaluation of the inclination effect is clearly a very complex problem. However, as this effect is small compared to typical inaccuracies of the N11 model, its inclusion in the model would not significantly alter the model performance, and we do not account for it. It is, nevertheless, a bit surprising that the main factor controlling the electron densities at higher altitudes is the crustal magnetic field strength, with the magnetic field orientation playing only a marginal role. It might be related to the inaccuracies of the used magnetic field inclinations based on the *Cain et al.* [2003] magnetic field model evaluated at a fixed altitude of 400 km. Moreover, the spatial scales of the density variations due to the crustal magnetic field orientation may be rather small, making it difficult to evaluate them properly. However, as the crustal magnetic fields are typically more inclined than the nearly horizontal-induced magnetic fields, the vertical transport should be generally easier in regions of strong crustal magnetic fields. This likely explains larger electron densities observed in these regions at higher altitudes. Finally, localized crustal magnetic fields can be strong enough to stand off the solar wind and create mini magnetospheres above the surface [*Krymskii et al.*, 2004; *Mitchell et al.*, 2001].

The suggested way of accounting for the crustal magnetic field magnitude effects (equation (3)) successfully removes the variation at altitudes between the peak altitude and 325 km. We note that the fit dependence was chosen purely because of its good performance within the investigated range of parameters, with no physical reasons of why it should be the correct form of the relationship. The used data set does not allow us to investigate the behavior at higher altitudes. Nevertheless, the results obtained by *Andrews et al.* [2015] indicate that at altitudes higher than 325 km one should also consider the variation of the diffusion scale height with the magnetic field magnitude (while the N11 model parameterizes the diffusion scale height only by the solar zenith angle).

The N11 model accounted for the varying $F_{10.7}$ solar ionizing flux at altitudes close to the altitude of the peak electron density, but the electron densities in the high-altitude diffusion region were not parameterized by $F_{10.7}$. We showed that this can lead to more than a factor of 2 difference at an altitude of 325 km. The suggested modification of the N11 model successfully accounts for this variation. However, two points should be stressed in this regard. First, $F_{10.7}$ is only a proxy for the solar ionizing flux, and it performs rather poorly especially for high values of $F_{10.7}$ [*Girazian and Withers*, 2013]. It is, however, easily available, and it is thus still a favorite choice to parameterize simple empirical models like N11. Second, the correction factor that we suggest (equation (4)) is clearly a physically incorrect dependence, as it can be seen from the negative values that it would provide for low $F_{10.7}$. Nevertheless, the suggested correction factor performs well in the analyzed range of $F_{10.7}$ values (approximately $25-65 \times 10^{-22}$ W m^{-2} Hz^{-1}), i.e., within the entire range sampled so far by the Mars Express spacecraft.

The analysis of selected reliable electron density profiles ranging from the peak altitudes up to the altitude of 325 km confirmed that the N11 model performs well at altitudes close to the altitude of the ionospheric peak. At higher altitudes, both the varying crustal magnetic field magnitude and the varying solar ionizing flux lead to median differences as large as a factor of 2. The suggested simple modifications (equations (3) and (4)) successfully account for these variations. The revised N11 model provides a simple, fast, and at least on average very accurate description of electron densities in the Martian dayside ionosphere. The model performance close to the ionospheric peak was thoroughly discussed by *Němec et al.* [2011]. The distribution of measured to model electron densities at an altitude of 325 km calculated using the revised model resembles

a Gaussian distribution. It has a standard deviation of about 0.4, and the difference between the 0.75 and 0.25 quartiles is about 0.5. Formerly present systematic biases at higher altitudes discussed in the present paper were successfully removed.

The significant scatter of the measured electron densities around the mean dependencies predicted by the model indicates that there remains a number of parameters and/or physical processes which were not taken into account. These may include (but certainly are not limited to) temperature variations as a function of the location, effects of dust storms, variations in the solar wind parameters, transient events in the solar wind, and, importantly, variations related to the solar cycle. According to a recent work by *Sánchez-Cano et al.* [2015], the ionospheric behavior during the period of extremely low solar activity is different than in other phases of the solar cycle. Specifically, they reported that during the solar minimum the topside total electron content was low and principally independent on the solar ionizing flux. On the other hand, our model assumes the same $F_{10.7}$ dependence for all phases of the solar cycle. This might possibly explain the large discrepancy between the N11 model and observations during the lowest levels of solar activity in Figure 6 (dark blue curve at the very left). Although this discrepancy is significantly reduced in the revised version of the model (Figure 8b), it is still clearly observable, in particular at the middle altitudes.

5. Conclusions

We have used 12,665 electron density profiles obtained by the MARSIS instrument since August 2005 until the end of 2013 to investigate the effects of possible control parameters unconsidered in the N11 empirical model. We have shown that while the peak density and altitude are nearly unaffected by crustal magnetic fields, electron densities at higher altitudes are significantly larger in areas of stronger magnetic fields. The magnetic field inclination has only a marginal effect, both at low and higher altitudes. We also investigated the influence of $F_{10.7}$ on the high-altitude region, which was parameterized only by the solar zenith angle and the altitude in the N11 model. We showed that the influence of $F_{10.7}$ at high altitudes is, nevertheless, rather significant. We suggested a simple correction of the N11 model, which takes into account both the crustal magnetic field magnitude and the effect of $F_{10.7}$ at higher altitudes. The Interactive Data Language source code of the revised N11 model can be downloaded from/run online at http://nemec.matfyz.cz/n11.

Acknowledgments
MARSIS data are available via the ESA Planetary Science Archive (http://www.rssd.esa.int/PSA). This work was supported by the KONTAKT II grant LH13031. The research at the University of Iowa was supported by NASA through contract 1224107 with the Jet Propulsion Laboratory.

References

Andrews, D. J., H. J. Opgenoorth, N. J. T. Edberg, M. André, M. Fränz, E. Dubinin, F. Duru, D. Morgan, and O. Witasse (2013), Determination of local plasma densities with the MARSIS radar: Asymmetries in the high-altitude Martian ionosphere, *J. Geophys. Res. Space Physics*, *118*, 6228–6242, doi:10.1002/jgra.50593.

Andrews, D. J., N. J. T. Edberg, A. I. Eriksson, D. A. Gurnett, D. Morgan, F. Němec, and H. J. Opgenoorth (2015), Control of the topside Martian ionosphere by crustal magnetic fields, *J. Geophys. Res. Space Physics*, *120*, 3042–3058, doi:10.1002/2014JA020703.

Brain, D. A., F. Bagenal, M. H. Acuña, and J. E. P. Connerney (2003), Martian magnetic morphology: Contributions from the solar wind and crust, *J. Geophys. Res.*, *108*(A12), 1424, doi:10.1029/2002JA009482.

Breus, T. K., A. M. Krymskii, D. H. Crider, N. F. Ness, D. Hinson, and K. K. Barashyan (2004), Effects of the solar radiation in the topside atmosphere/ionosphere of Mars: Mars Global Surveyor observations, *J. Geophys. Res.*, *109*, A09310, doi:10.1029/2004JA010431.

Cain, J. C., B. B. Ferguson, and D. Mozzoni (2003), An $n = 90$ internal potential function of the Martian crustal magnetic field, *J. Geophys. Res.*, *108*(E2), 5008, doi:10.1029/2000JE001487.

Chapman, S. (1931a), The absorption and dissociative or ionizing effect of monochromatic radiation in an atmosphere on a rotating Earth, *Proc. Phys. Soc. London*, *43*, 26–45.

Chapman, S. (1931b), The absorption and dissociative or ionizing effect of monochromatic radiation in an atmosphere on a rotating Earth. Part II. Grazing incidence, *Proc. Phys. Soc. London*, *43*, 483–501.

Chicarro, A., P. Martin, and R. Trautner (2004), The Mars Express mission: An overview, in *Mars Express: The Scientific Payload, ESA Spec. Publ.*, vol. 1240, edited by A. Wilson and and A. Chicarro, pp. 3–13, ESA Publ. Div., Noordwijk, Netherlands.

Cui, J., M. Galand, S. J. Zhang, E. Vigren, and H. Zou (2015), The electron thermal structure in the dayside Martian ionosphere implied by the MGS radio occultation data, *J. Geophys. Res. Planets*, *120*, 278–286, doi:10.1002/2014JE004726.

Duru, F., D. A. Gurnett, T. F. Averkamp, D. L. Kirchner, R. L. Huff, A. M. Persoon, J. J. Plaut, and G. Picardi (2006), Magnetically controlled structures in the ionosphere of Mars, *J. Geophys. Res.*, *111*, A12204, doi:10.1029/2006JA011975.

Duru, F., D. A. Gurnett, D. D. Morgan, R. Modolo, A. F. Nagy, and D. Najib (2008), Electron densities in the upper ionosphere of Mars from the excitation of electron plasma oscillations, *J. Geophys. Res.*, *113*, A07302, doi:10.1029/2008JA013073.

Duru, F., D. A. Gurnett, D. D. Morgan, J. D. Winningham, R. A. Frahm, and A. F. Nagy (2011), Nightside ionosphere of Mars studied with local electron densities: A general overview and electron density depressions, *J. Geophys. Res.*, *116*, A10316, doi:10.1029/2011JA016835.

Fallows, K., P. Withers, and M. Matta (2015a), An observational study of the influence of solar zenith angle on properties of the M1 layer of the Mars ionosphere, *J. Geophys. Res. Space Physics*, *120*, 1299–1310, doi:10.1002/2014JA020750.

Fallows, K., P. Withers, and M. Matta (2015b), Numerical simulations of the influence of solar zenith angle on properties of the M1 layer of the Mars ionosphere, *J. Geophys. Res. Space Physics*, *120*, 6707–6721, doi:10.1002/2014JA020947.

Fox, J. L., and A. J. Weber (2012), MGS electron density profiles: Analysis and modeling of peak altitudes, *Icarus*, *221*, 1002–1019, doi:10.1016/j.icarus.2012.10.002.

Fox, J. L., and K. E. Yeager (2009), MGS electron density profiles: Analysis of the peak magnitudes, *Icarus*, *200*, 468–479, doi:10.1016/j.icarus.2008.12.002.
Girazian, Z., and P. Withers (2013), The dependence of peak electron density in the ionosphere of Mars on solar irradiance, *Geophys. Res. Lett.*, *40*, 1960–1964, doi:10.1002/grl.50344.
Grandin, M., P.-L. Blelly, O. Witasse, and A. Marchaudon (2014), Mars Express radio-occultation data: A novel analysis approach, *J. Geophys. Res. Space Physics*, *119*, 10,621–10,632, doi:10.1002/2014JA020698.
Gurnett, D. A., et al. (2005), Radar soundings of the ionosphere of Mars, *Science*, *310*, 1929–1933.
Gurnett, D. A., et al. (2008), An overview of radar soundings of the martian ionosphere from the Mars Express spacecraft, *Adv. Space Res.*, *41*, 1335–1346.
Hinson, D. P., R. A. Simpson, J. D. Twicken, G. L. Tyler, and F. M. Flasar (1999), Initial results from radio occultation measurements with Mars Global Surveyor, *J. Geophys. Res.*, *104*(E11), 26,997–27,012, doi:10.1029/1999JE001069.
Jordan, R., et al. (2009), The Mars Express MARSIS sounder instrument, *Planet. Space Sci.*, *57*, 1975–1986, doi:10.1016/j.pss.2009.09.016.
Kopf, A. J., D. A. Gurnett, D. D. Morgan, and D. K. Kirchner (2008), Transient layers in the topside ionosphere of Mars, *Geophys. Res. Lett.*, *35*, L17102, doi:10.1029/2008GL034948.
Krymskii, A. M., N. F. Ness, D. H. Crider, T. K. Breus, M. H. Acuña, and D. P. Hinson (2004), Solar wind interaction with the ionosphere/atmosphere and crustal magnetic fields at Mars: Mars Global Surveyor Magnetometer/Electron Reflectometer, radio science, and accelerometer data, *J. Geophys. Res.*, *109*, A11306, doi:10.1029/2004JA010420.
Matta, M., M. Mendillo, P. Withers, and D. Morgan (2015), Interpreting Mars ionospheric anomalies over crustal magnetic field regions using a 2-D ionospheric model, *J. Geophys. Res. Space Physics*, *120*, 766–777, doi:10.1002/2014JA020721.
Mendillo, M., A. Lollo, P. Withers, M. Matta, M. Pätzold, and S. Tellmann (2011), Modeling Mars' ionosphere with constraints from the same-day observations by Mars Global Surveyor and Mars Express, *J. Geophys. Res.*, *116*, A11303, doi:10.1029/2011JA016865.
Mendillo, M., A. G. Marusiak, P. Withers, D. Morgan, and D. Gurnett (2013), A new semiempirical model of the peak electron density of the Martian ionosphere, *Geophys. Res. Lett.*, *40*, 5361–5365, doi:10.1002/2013GL057631.
Mitchell, D. L., R. P. Lin, C. Mazelle, H. Rème, P. A. Cloutier, J. E. P. Connerney, M. H. Acunña, and N. F. Ness (2001), Probing Mars' crustal magnetic field and ionosphere with the MGS electron reflectometer, *J. Geophys. Res.*, *106*(E10), 23,419–23,427.
Morgan, D. D., D. A. Gurnett, D. L. Kirchner, J. L. Fox, E. Nielsen, and J. J. Plaut (2008), Variation of the Martian ionospheric electron density from Mars Express radar soundings, *J. Geophys. Res.*, *113*, A09303, doi:10.1029/2008JA013313.
Morgan, D. D., O. Witasse, E. Nielsen, D. A. Gurnett, F. Duru, and D. L. Kirchner (2013), The processing of electron density profiles from the Mars Express MARSIS topside sounder, *Radio Sci.*, *48*, 197–207, doi:10.1002/rds.20023.
Nagy, A. F., et al. (2004), The plasma environment of Mars, *Space Sci. Rev.*, *111*, 33–114.
Nielsen, E., X.-D. Wang, D. A. Gurnett, D. L. Kirchner, R. Huff, R. Orosei, A. Safaeinili, J. J. Plaut, and G. Picardi (2007a), Vertical sheets of dense plasma in the topside Martian ionosphere, *J. Geophys. Res.*, *112*, E02003, doi:10.1029/2006JE002723.
Nielsen, E., et al. (2007b), Local plasma processes and enhanced electron densities in the lower ionosphere in magnetic cusp regions on Mars, *Planet. Space Sci.*, *55*, 2164–2172.
Němec, F., D. D. Morgan, D. A. Gurnett, and F. Duru (2010), Nightside ionosphere of Mars: Radar soundings by the Mars Express spacecraft, *J. Geophys. Res.*, *115*, E12009, doi:10.1029/2010JE003663.
Němec, F., D. D. Morgan, D. A. Gurnett, F. Duru, and V. Truhlík (2011), Dayside ionosphere of Mars: Empirical model based on data from the MARSIS instrument, *J. Geophys. Res.*, *116*, E07003, doi:10.1029/2010JE003789.
Pätzold, M., S. Tellmann, B. Häusler, D. Hinson, R. Schaa, and G. L. Tyler (2005), A sporadic third layer in the ionosphere of Mars, *Science*, *310*, 837–839, doi:10.1126/science.1117755.
Picardi, G., et al. (2004), MARSIS: Mars advanced radar for subsurface and ionosphere sounding, in *Mars Express: The Scientific Payload, ESA Spec. Publ.*, vol. 1240, edited by A. Wilson and and A. Chicarro, pp. 51–69, ESA, Noordwijk.
Riousset, J. A., C. S. Paty, R. J. Lillis, M. O. Fillingim, S. L. England, P. G. Withers, and J. P. M. Hale (2014), Electrodynamics of the Martian dynamo region near magnetic cusps and loops, *Geophys. Res. Lett.*, *41*, 1119–1125, doi:10.1002/2013GL059130.
Sánchez-Cano, B., O. Witasse, M. Herraiz, S. M. Radicella, J. Bauer, P.-I. Blelly, and G. Rodríguez-Caderot (2012), Retrieval of ionospheric profiles from the Mars Express MARSIS experiment data and comparison with radio occultation data, *Geosci. Instrum. Methods Data Syst.*, *1*, 77–84, doi:10.5194/gi-1-77-2012.
Sánchez-Cano, B., S. M. Radicella, M. Herraiz, O. Witasse, and G. Rodríguez-Caderot (2013), NeMars: An empirical model of the martian dayside ionosphere based on Mars Express MARSIS data, *Icarus*, *225*, 236–247, doi:10.1016/j.icarus.2013.03.021.
Sánchez-Cano, B., M. Lester, O. Witasse, S. E. Milan, B. E. S. Hall, P.-L. Blelly, S. M. Radicella, and D. D. Morgan (2015), Evidence of scale height variations in the Martian ionosphere over the solar cycle, *J. Geophys. Res. Space Physics*, *120*, 10,913–10,925, doi:10.1002/2015JA021949.
Schunk, R. W., and A. F. Nagy (2009), *Ionospheres*, 2nd ed., Cambridge Univ. Press, Cambridge, U. K., doi:10.1017/CBO9780511635342.
Tyler, G. L., G. Balmino, D. P. Hinson, W. L. Sjogren, D. E. Smith, R. A. Simpson, S. W. Asmar, P. Priest, and J. D. Twicken (2001), Radio science observations with Mars Global Surveyor: Orbit insertion through one Mars year in mapping orbit, *J. Geophys. Res.*, *106*(E10), 23,327–23,348.
Withers, P. (2009), A review of observed variability in the dayside ionosphere of Mars, *Adv. Space Res.*, *44*, 277–3078.
Withers, P., and M. Mendillo (2005), Response of peak electron densities in the martian ionosphere to day-to-day changes in solar flux due to solar rotation, *Planet. Space Sci.*, *53*, 1401–1418, doi:10.1016/j.pss.2005.07.010.
Withers, P., M. Mendillo, H. Rishbeth, D. P. Hinson, and J. Arkani-Hamed (2005), Ionospheric characteristics above Martian crustal magnetic anomalies, *Geophys. Res. Lett.*, *32*, L16204, doi:10.1029/2005GL023483.
Withers, P., et al. (2012), A clear view of multifaceted dayside ionosphere of Mars, *Geophys. Res. Lett.*, *39*, L18202, doi:10.1029/2012GL053193.